Desalination 540 (2022) 115995

Contents lists available at ScienceDirect

Desalination

journal homepage: www.elsevier.com/locate/desal

Design of novel seawater bittern recovery process for CO_2 and SO_x utilization

Jonghun Lim [a,b,1], Deok Ju Kim [a,c,1], Hyungtae Cho [a], Junghwan Kim [a,*]

[a] Green Materials and Processes R&D Group, Korea Institute of Industrial Technology, Ulsan 44413, Republic of Korea
[b] Department of Chemical and Biomolecular Engineering, Yonsei University, Seoul 03722, Republic of Korea
[c] Department of Chemical Engineering, Konkuk University, Seoul 05029, Republic of Korea

HIGHLIGHTS

- Seawater bittern was used to capture CO_2 and SO_x.
- The pay-back period was calculated to verify the feasibility of the proposed process.
- High SO_x and CO_2 capture efficiencies were obtained using the proposed method.

ARTICLE INFO

Keywords:
Salt production
Seawater bittern
CO_2 capture and utilization
SO_x capture and utilization

ABSTRACT

Considerable seawater bittern is produced during salt production. Seawater bittern can be used to reduce CO_2 and SO_x because of the presence of valuable mineral ions, such as K^+ and Mg^{2+}, which react with the carbonate and sulfate ions present in high concentrations. In this study, a novel seawater bittern recovery process is proposed for CO_2 and SO_x utilization. The proposed process has the following steps: (1) metal ion separation of the seawater bittern to produce KOH and $Mg(OH)_2$; (2) SO_x capture and utilization using the generated $Mg(OH)_2$; (3) CO_2 capture and utilization using the generated KOH. The pay-back period (PBP) was calculated to verify the economic feasibility of the proposed process. The results revealed an SO_x and a CO_2 capture efficiency of approximately 99 % and 98 %, respectively. Furthermore, the annual net revenue was approximately 153,439 USD/y based on the profit obtained from the generated product and savings on absorbent. Thus, the PBP was approximately 6.2 y.

1. Introduction

In many countries, seawater bitterns generated from salt production facilities are directly discarded [1]. Sea salts are produced when the sea water undergoes several procedures, such as stabilization, evaporation, concentration, and crystallization [2]. Seawater bittern is a concentrated solution that still exists after the salt crystallization process; it is rich in Mg2+ and contains various other metal ions [3]. In South Korea, seawater bittern of approximately 100,000 ton is annually discarded during salt harvesting, storage, and manufacturing [4]. Since the discarded seawater bittern contains high concentrations of inorganic substances, such as K^+ and Mg^{2+} ions, which react with carbonate and sulfate ions and thus, seawater bittern can be used for CO_2 and SO_x capture and utilization [3]. However, direct discharge of seawater bittern causes considerable environmental pollution, ecosystem destruction, and economic losses. The huge amount of discharged seawater bittern has an adverse impact on the aquatic life [2]. Thus, with regard to environmental sustainability, certain approaches such as ammonia nitrogen removal have been proposed for better disposal of seawater bittern [5].

Therefore, seawater bittern recycling has attracted considerable attention among researchers as an alternative to the disposal approach. Numerous methods have been proposed for efficient utilization of the mineral ions present in seawater bittern. Chandra et al. addressed the issue of KNO_3 recovery from seawater bittern [6]. They used $NaNO_3$ to recover the KNO_3, and 96.26 % of KNO_3, 97.19 % of NaCl, and 98.93 % of $MgCl_2{\cdot}6H_2O$ was recovered through the process of continued evaporation. Jumaeri et al. focused on the recovery of NaCl that still exists

* Corresponding author.
E-mail address: kjh31@kitech.re.kr (J. Kim).
[1] These authors contributed equally as first authors.

https://doi.org/10.1016/j.desal.2022.115995
Received 8 May 2022; Received in revised form 2 July 2022; Accepted 19 July 2022
Available online 4 August 2022

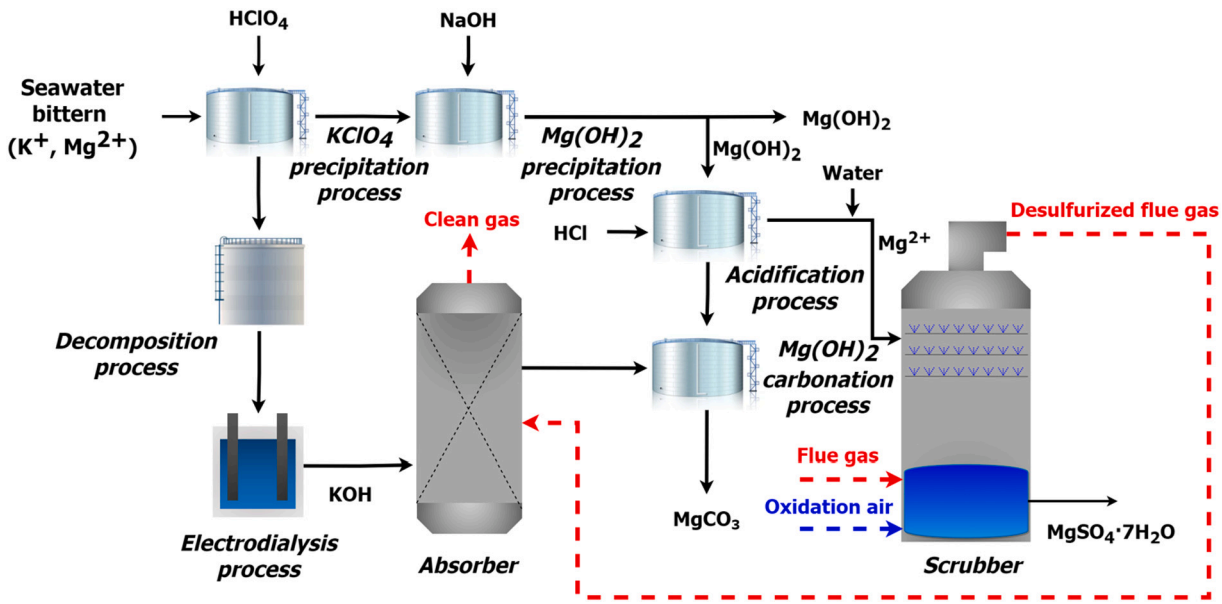

Fig. 1. Overview of the proposed process.

after the salt production, and the NaCl was recovered through the precipitation method with NaOH and evaporation [7]. As a result, 98.75 wt % of NaCl was recovered and the yield was determined to be 30.45 %. Amrulloh et al. synthesized $Mg(OH)_2$ from seawater bittern using the electrochemical method [8]. Thereafter, they used the synthesized $Mg(OH)_2$ for the removal of Pb(II) and Cd(II) ions from seawater bittern, and the adsorption kinetics followed the pseudo-second-order model with a rate constant of 2.27×10^{-5} and 2.52×10^{-5} g/mg·min for Pb(II) and Cd(II), respectively. Nalajala et al. recovered the $MgCl_2$ in seawater bitterns using spray and thermal drying [9]. They recovered 57.58–52.73 % of $MgCl_2$ at a flow rate of 2–5 mL/min. Sahu et al. developed a novel process for Na_2SO_4 recovery from seawater bittern. Their process comprised three stages: cooling crystallization, filtration, and drying, and the pay-back period of the developed process was determined to be 3.5 y [10]. Using the above process, they could recover 97 wt% of Na_2SO_4.

Among them, a study focused on the use of seawater bittern as a source for magnesium and an absorbent for CO_2 to reduce greenhouse gas emissions [11]. Furthermore, the effective use of seawater bittern for carbon capture and utilization (CCU) was investigated. The proposed process is composed of the following two procedures: (1) $Mg(OH)_2$ recovery through precipitation; (2) CO_2 capture through residual bittern after $Mg(OH)_2$ recovery. First, in $Mg(OH)_2$ recovery through precipitation, seawater bittern is mixed with NaOH to obtain precipitates of $Mg(OH)_2$. Next, the generated $Mg(OH)_2$ is commercialized. Second, CO_2 is captured using the residual bittern as a liquid-phase CO_2 absorbent and NH_4OH solution after $Mg(OH)_2$ recovery. Therefore, $NaHCO_3$ produced can be commercialized.

Although numerous studies have focused on the use of seawater bittern for CCU, the following major challenges remain. First, in previous studies, SO_x capture and utilization (SCU) has not been considered, and SO_x was already treated. In conventional SCUs, $CaCO_3$ is used as the SO_x absorbent to obtain limestone [12–14]. SO_x is captured through liquid–gas contact with the SO_x-containing flue gas and alkaline slurry, which is formed from pulverized limestone. Limestone should exhibit $CaCO_3$ purity of more than 94 wt% (i.e., high-grade limestone) because the other substances such as SiO_2 and Al_2O_3 decrease the purity of the desulfurization gypsum, which is a by-product of SCU [15]. However, high-grade limestone reserves are only 20 % of the total reserves [14]. Thus, a substitute of high-grade limestone is required. Second, in SCU using $CaCO_3$, CO_2 is inevitably emitted for SO_x removal; thus, there is increased greenhouse gas emission and the overall reaction proceeds as follows.

$$CaCO_3\ (s) + SO_2\ (g) \rightarrow CaSO_3\ (s) + CO_2\ (g) \tag{1}$$

It is not reasonable to use the conventional desulfurization method because the generated CO_2 is expected to be captured by the CCU process. Lime (CaO) is also used as an SO_x absorbent and does not emit CO_2; however, $CaCO_3$ sintering is required at high temperatures, which entails additional combustion of fossil fuels and increases cost. Finally, in seawater bittern, numerous K^+ ions exist, which can be used as an absorbent for capturing CO_2. However, additional NaOH is typically used for CO_2 capture. KOH and NaOH exhibit alkalinity and react with CO_2 through acid–base reaction; thus, they exhibit a high CO_2 capture efficiency. However, when the CO_2 absorption rate of 1–5 % NaOH solution reaches a range of 2.06–2.08 mg, the NaOH starts emitting CO_2 rather than absorbing it [16]. NaOH is converted to $NaHCO_3$ during CO_2 capture using NaOH. Based on the phase equilibrium, CO_2 is re-emitted from $NaHCO_3$ after a certain limit of CO_2 isolation. By contrast, KOH exhibits uniform CO_2 absorption. CO_2 is neutralized according to the zwitterion mechanism, involving direct absorption and conversion, in which KOH continuously absorbs CO_2 by the counter action of K^+ ions [17]. Therefore, using K^+ ions in seawater bittern is more feasible than the use of additional NaOH for CO_2 capture.

To address these problems, we proposed a novel seawater bittern recovery process for capturing CO_2 and SO_x. CCU and SCU systems were integrated, and Mg^{2+} and K^+ in seawater bittern were used to capture CO_2 and SO_x. The objective of the proposed method was to overcome the challenges of the conventional methods for capturing CO_2 and SO_x for environmental protection. The use of seawater bittern for CO_2 and SO_x capture has the following environmental and economic advantages over conventional previous studies:

1) The use of seawater bittern substitutes the use of conventional SO_x absorbents, such as high-grade limestone. Furthermore, because the additional expense for acquiring $CaCO_3$ is mitigated, the cost incurred in limestone mining is reduced and the generated $MgSO_4{\cdot}7H_2O$ and $MgCO_3$ can be sold.
2) $Mg(OH)_2$ generated from the metal ions in seawater bittern is used in the SCU system, which is a carbon-neutral desulfurization method. Thus, additional CO_2 generation is avoided. The simple desulfurization reaction using $Mg(OH)_2$ proceeds as follows:

$$Mg^{2+}(aq) + 2OH^{-}(aq) + SO_2\ (g) + 0.5\ O_2\ (g) \rightarrow MgSO_4(s) + H_2O(l) \quad (2)$$

3) Finally, because KOH generated from the seawater bittern is used for CO_2 capture, the CO_2 capture efficiency can be increased considerably over that using NaOH without any additional CO_2 emission caused by phase equilibrium.

The contributions of this study are summarized as follows:

1) This study is the first to simultaneously enable CCU and SCU using seawater bittern.
2) In the proposed process, metal ions in seawater bittern are used for CCU and SCU. Therefore, it is an environment-friendly method of mitigating pollution caused by waste seawater bittern and overcoming feedstock restrictions of conventional absorbents.
3) In this study, an environmental and economical approach was proposed to capture and utilize CO_2 and SO_x in the flue gas emitted from power plants using only seawater bittern that is generally discharged.

2. Methodology

2.1. Overview of the suggested seawater bittern recovery process

Fig. 1 displays an overview of the proposed process: (1) metal ion separation of the seawater bittern; (2) SO_x capture and utilization through $Mg(OH)_2$; (3) CO_2 capture and utilization using KOH.

2.1.1. Step 1. Metal ion separation of seawater bittern

In metal ion separation of seawater bittern, first, K^+ ions are separated based on the difference in solubility of each metal ion at various pH levels. By adding $HClO_4$ to seawater bittern during the $KClO_4$ precipitation process, $KClO_4$ is precipitated and subsequently decomposed to KCl, which is used for the chlor-alkali electro dialysis process. $KClO_4$ precipitates first because the solubility of $Mg(ClO_4)_2$, which is generated when $HClO_4$ is added to seawater bittern, is significantly greater than that of $KClO_4$. Next, the generated KCl is converted to KOH using the chlor-alkali electro dialysis process. KOH is used to capture and utilize CO_2. Second, Mg^{2+} ions are separated by adding NaOH to seawater bittern because K^+ ions are separated, and $Mg(OH)_2$ is selectively precipitated between pH 7 and 11. In this study, pH was set between 9.5 and 10 to maximize $Mg(OH)_2$ separation.

2.1.2. Step 2. SO_x capture and utilization

$Mg(OH)_2$ formed during the metal ion separation process of the seawater bittern is used to capture and utilize SO_x. Because $Mg(OH)_2$ is insoluble in pure water, to increase its reactivity with SO_x, HCl is added to the $Mg(OH)_2$ solution in an acidification process before generating alkaline slurry. In the acidification process, $Mg(OH)_2$ is ionized by reacting it with HCl. Next, alkaline slurry is generated by adding water to ionized $Mg(OH)_2$ and spraying it at the top of the scrubber. The flue gas comes in contact with the alkaline slurry and SO_x is captured as a result of the vapor–liquid contact. Finally, in the liquid phase at the bottom of the scrubber, $MgSO_4{\cdot}7H_2O$(i.e., epsom salt) is generated, and the desulfurized flue gas is emitted on to the absorber for CO_2 capture and utilization.

2.1.3. Step 3. CO_2 capture and utilization

Finally, CO_2 in desulfurized flue gas is captured and utilized using the generated KOH at the absorber. Next, captured CO_2 exists in the ionic rich flow, which contains HCO_3^- and CO_3^{2-}, and the rich flow reacts with Mg^{2+} ions at the $Mg(OH)_2$ carbonation process generating $MgCO_3$. After SO_x and CO_2 capture process, the generated $MgSO_4{\cdot}7H_2O$ and $MgCO_3$ are utilized.

2.2. Thermal dynamic and ion balance model

2.2.1. Thermal dynamic model

In this study, the electrolyte nonrandom two-liquid thermal dynamic model was used to model the proposed process. The ELECNTL model is the most versatile electrolyte method in which the modified NRTL and Pitzer–Debye–Huckle models are combined to consider the ionic interaction of the vapor–liquid and liquid–liquid equilibriums as follows [2,3]:

$$ln\gamma_i = \frac{\sum_{j=1}^{m} x_j \tau_{ji} G_{ji}}{\sum_{l=1}^{m} x_l G_{li}} + \sum_{j=1}^{m} \frac{x_j G_{ij}}{\sum_{l=1}^{m} x_l G_{lj}} \left(\tau_{ij} - \frac{\sum_{r=1}^{m} x_r \tau_{rj} G_{rj}}{\sum_{l=1}^{m} x_l G_{lj}} \right) \quad (3)$$

$$ln\gamma_i = ln\gamma_i^{local} + ln\gamma_i^{PDH} \quad (4)$$

$$ln\gamma_i^{local} = \frac{1}{RT}\left(\frac{\partial G_m^{ex,local}}{\partial n_i}\right)_{T,P,n_j \neq i};\ ln\gamma_i^{PDH} = \frac{1}{RT}\left(\frac{\partial G_m^{ex,PDH}}{\partial n_i}\right)_{T,P,n_j \neq i} \quad (5)$$

where, γ_i = *activity coefficienct of component i*; $G_{ij} = exp\ [-\tau_{ij}\alpha_{ij}]$; $\tau_{ij} = \frac{a_{ij}+b_{ij}T}{RT}$; x_i = *mole fraction of component i*; T = *temperature (K)*; m = *total number of components*; a_{ij} = *temperature − independent energy parameter between components i and j (cal/gmol · K)*; b_{ij} = *temperature − dependent energy parameter between components i and j (cal/gmol · K)*; and α_{ij} = *NRTL non − randomness constant for binary interaction (note that $\alpha_{ij} = \alpha_{ji}$ for all binaries)*.

The following gas phase expression of the Redlich–Kwong state equation is used:

$$P = \frac{RT}{V_m - b} - \frac{a/T^{0.5}}{V_m(V_m + b)} \quad (6)$$

where, $a = 0.42748\frac{R^2T_c^{2.5}}{P_c}$; and $b = 0.08664\frac{RT_c}{P_c}$.

2.2.2. Ion balance model

To simulate the chlor-alkali electrolysis process that generates NaOH and KOH, the following ion balance model is used [20]:

$$\frac{dN_{CatAcc}^{Na}}{dt} = C_{CatIn}^{NaOH} \cdot \dot{V}_{CatIn} - C_{CatAcc}^{Na} \cdot \dot{V}_{CatOut} + \frac{A \cdot D^{Na}}{\delta} \cdot \left(C_{AnAcc}^{Na} - C_{CatAcc}^{Na}\right) \quad (7)$$

$$\frac{dN_{AnAcc}^{Na}}{dt} = C_{AnIn}^{NaCl} \cdot \dot{V}_{AnIn} - C_{AnAcc}^{Na} \cdot \dot{V}_{AnOut} + \frac{A \cdot D^{Na}}{\delta} \cdot \left(C_{AnAcc}^{Na} - C_{CatAcc}^{Na}\right) \quad (8)$$

$$C_{AnIn}^{Na} = \frac{N_{AnAcc}^{Na}}{V_{AnAcc}};\ C_{CatIn}^{Na} = \frac{N_{CatAcc}^{Na}}{V_{CatAcc}} \quad (9)$$

where,

N_{CatAcc}, N_{AnAcc} = *mole quantity in the catholyte and anolyte (kmol)*;
C_{CatIn}, C_{AnIn} = *concentration in the catholyte feed and anolyte feed ($kmol/m^3$)*;
C_{CatAcc}, C_{AnAcc} = *concentration in the catholyte and anolyte ($kmol/m^3$)*;
$\dot{V}_{CatIn}$, $\dot{V}_{AnIn}$ = *volume rate of the cathode inlet and anode inlet (m^3/s)*;
$\dot{V}_{CatOut}$, $\dot{V}_{AnOut}$ = *volume rate of the cathode outlet and anode outlet (m^3/s)*;
A = *ion diffusion area in the membrane (m^2)*;
D = *diffusion coefficient (m^2/s); and*
δ = *membrane thickness (m)*.

The OH^- ion is generated by the cathode reaction, which separates water to produce OH^- and H^+ ions. According to Faraday's law, the OH^- production rate is in proportion to the current intensity [20]:

$$\frac{dN_{CatAcc}^{OH}}{dt} = C_{CatIn}^{NaOH} \cdot \dot{V}_{CatIn} + \frac{i \cdot A_{el}}{2F} - \frac{N_{CatAcc}^{OH}}{V_{CatAcc}} \cdot \dot{V}_{CatOut} \quad (10)$$

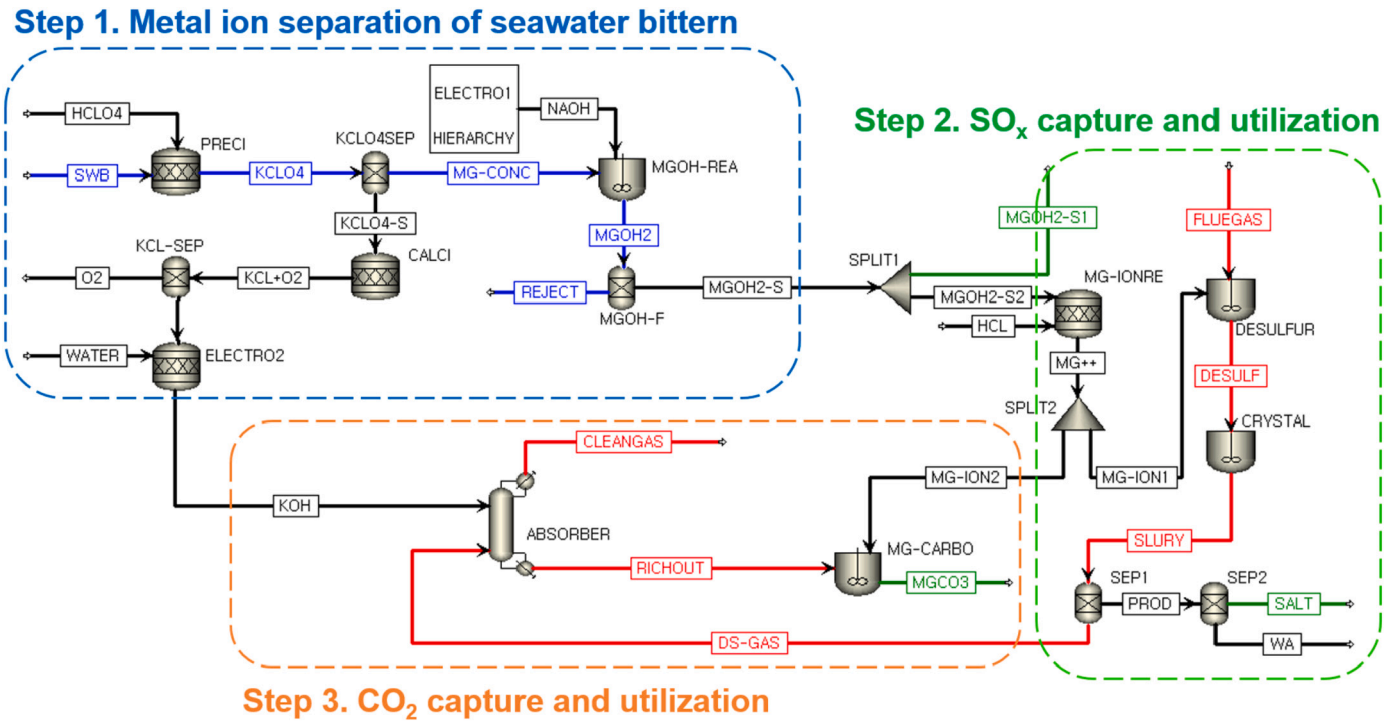

Fig. 2. Process model of the proposed seawater bittern recovery process.

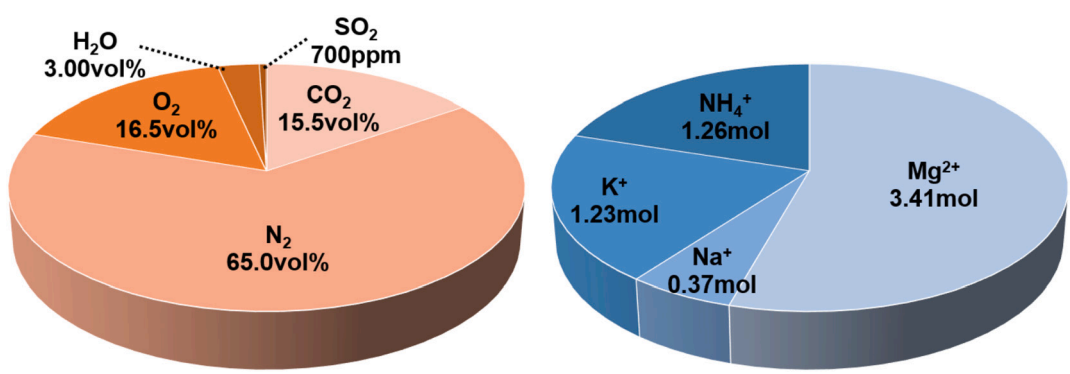

Fig. 3. Flue gas composition (left) and molarity of metal cations in seawater bittern (right).

Subsequently, saturated NaCl was used to produce KOH in the electrolysis chamber. K^+ ion was moved to the cathode chamber through the membrane, and Cl^- ion was oxidized in the anode chamber and converted to Cl_2 as follows [20]:

$$\frac{dN_{AnAcc}^{OH}}{dt} = C_{AnIn}^{NaCl} \cdot \dot{V}_{AnIn} - \frac{i \cdot A_{el}}{2F} - \frac{N_{AnAcc}^{OH}}{V_{AnAcc}} \cdot \dot{V}_{AnOut} \tag{11}$$

2.3. Process model

Fig. 2 displays the process model of the proposed seawater bittern recovery process. Aspen Plus V11.0 is used and the electrolysis process is simulated using MATLAB® version R2020b from MathWorks. The following assumptions are considered to develop the process model:

- The process is in a steady state.
- Rate-based models are used for columns with packing.
- The top stage pressure is provided for column convergence.
- The flow rate of flue gas is 0.57 kmol/h.
- The flow rate of seawater bittern is 8.9 kmol/h.
- Flue gas composition is considered according to the method proposed by Meunier et al. [21], and metal cations' molarity in 1 L of seawater bittern is considered based on the study by Kuda et al. [3] (Fig. 3).
- The flue gas only contains CO_2, N_2, O_2, H_2O, and SO_x, and it is assumed that NO_x is already treated.
- The Mg/S ratio is set as 1.6 [22].

2.3.1. Metal ion separation

In seawater bittern, Mg^{2+} and K^+ exhibit high capture efficiency for SO_x and CO_2. First, to separate K^+ ions, $HClO_4$ (HCLO4) is added to seawater bittern (SWB); $KClO_4$ (KCLO4), which exhibits the lowest solubility of any alkali metal perchlorate at 25 °C, is precipitated based on the solubility difference with the perchlorate and each metal ion.

$$K^+ + HClO_4 \rightarrow H^+ + KClO_4 \downarrow \tag{12}$$

The solubility of $KClO_4$, $Mg(ClO_4)_2$, and $Na(ClO_4)_2$ in water is 1.5 g/100 mL, 99.3 g/100 mL, and 209.6 g/100 mL, respectively [23]. The precipitation rate of $KClO_4$ is determined by the temperature and pH

level. In this study, the temperature and the pH level are set to −7 °C and 2, respectively, according to a study performed by Chen et al. To model the $KClO_4$ precipitation process (PRECI), the RSTOIC model is used. Based on the experimental precipitation rate of $KClO_4$ under aforementioned conditions, the conversion rate of $KClO_4$ is set to 99.92 % [24]. Next, the generated $KClO_4$ is decomposed using the decomposition process (CALCI) to produce KCl, which is used for the electrodialysis process. To model the $KClO_4$ decomposition process, the RSTOIC model is used and the decomposition rate is set to 99.5 %. The following equation is specified by the RSTOIC model to simulate the decomposition process, and the conversion rate of KCl is set to 99.5 %.

$$KClO_4 \rightarrow \Delta KCl + 2O_2\uparrow \tag{13}$$

The generated KCl (KCL + O2) is used in the electrolysis process to produce KOH (ELECTRO2), which is used as a CO_2 absorbent. The K^+ ions in seawater bittern are separated through the $KClO_4$ precipitation process. The generated Mg^{2+} ions can be used for SO_x capture. However, other metal ions, such as NH_4^+ ions, in seawater bittern interrupt SO_x capture. The following physical and chemical side reactions occur for the forward reaction between and SO_x, which reduces SO_x capture efficiency. Therefore, separating Mg^{2+} ions is necessary and can be achieved using the following process [25]:

$$Mg(OH)_2 + 2NH_4^+ \rightarrow Mg^{2+} + 2NH_3 + 2H_2O \tag{14}$$

Therefore, to separate Mg^{2+} ions in seawater bittern, NaOH (NAOH) is added, and Mg^{2+} is separated as a form of $Mg(OH)_2$ at the $Mg(OH)_2$ precipitation process (MGOH-REA). To model the $Mg(OH)_2$ precipitation process, the RCSTR model is used, and the equilibrium constant is set based on Gibbs free energy minimization. The equation which is considered in MGOH-REA is as follows [25]:

$$Mg^{2+} + 2OH^- \leftrightarrow Mg(OH)_2 \tag{15}$$

The separated $Mg(OH)_2$ (MGOH2-S) is used in SO_x capture and $Mg(OH)_2$ carbonation processes. In seawater bittern, Mg^{2+} ions are abundant, which results in considerable amounts of $Mg(OH)_2$. Thus, if the generated $Mg(OH)_2$ exceed the required amount for SO_x capture, it can be commercialized to generate economic profits. The generated $Mg(OH)_2$ exhibits a purity of 94 wt%, and can be used in products such as antacid and laxatives [4].

2.3.2. Electrolysis

NaOH and KOH are produced during the electrolysis process of NaCl (ELECTRO1) and KCl (ELECTRO2). To model the electrolysis process and consider the ion behavior at the anode and cathode, MATLAB® version R2020b from MathWorks was used as dynamic simulation software. The electrolysis reactions at the anode and cathode cells are as follows [26]:

$$2Na^+(or\ 2K^+) + 2Cl^- \rightarrow Cl_2 + 2Na^+(or\ 2K^+) + 2e^- \tag{16}$$

$$2Cl^- \rightarrow Cl_2 + 2e^- \tag{17}$$

$$2H_2O + 2e^- \rightarrow H_2 + OH^- \tag{18}$$

$$\mathrm{Na}^+(or\ K^+) + OH^- \rightarrow NaOH(or\ KOH) \tag{19}$$

$$2H_2O + 2NaCl(or\ 2KCl) \rightarrow H_2 + Cl_2 + 2NaOH(or\ 2KOH) \tag{20}$$

Next, the generated NaOH is used as a buffer solution to precipitate $Mg(OH)_2$, and KOH is used for CO_2 capture.

2.3.3. SO_x capture and utilization

To capture SO_x, the $Mg(OH)_2$ separated from seawater bittern is used for wet flue gas desulfurization. Since the reacting phases of the top and bottom surfaces of the scrubber are different, the scrubber is modeled in the following two steps: (1) top of the scrubber, which is a gas–liquid phase (DESULFUR); (2) bottom of the scrubber, which is a liquid phase (CRYSTAL).

To model the scrubber, the RCSTR model is used and the equilibrium constants are considered based on the Gibbs free energy minimization. Because $Mg(OH)_2$ is insoluble in pure water, to increase reactivity with SOx, HCl is added to the $Mg(OH)_2$ solution during the acidification process before generating alkaline slurry. In the acidification process, $Mg(OH)_2$ is ionized by reacting with HCl as follows [22]:

$$Mg(OH)_2 + 2HCl \rightarrow MgCl_2(aq) + 2H_2O \tag{21}$$

Next, alkaline slurry is generated by ionizing $Mg(OH)_2$ via addition of water and spraying it at the top of the scrubber. The flue gas comes in contact with alkaline slurry, and SO_x is captured because of the vapor–liquid contact as follows [27]:

$$SO_2 + H_2O \leftrightarrow H_2SO_3 \tag{22}$$

$$H_2SO_3 \leftrightarrow H^+ + HSO_3^- \tag{23}$$

$$HSO_3^- + 0.5O_2 \leftrightarrow H^+ + SO_4^{2-} \tag{24}$$

Finally, in the liquid phase at the bottom of the scrubber, $MgSO_4{\cdot}7H_2O$, which is also called Epsom salt (SALT), is generated and the remaining water (WA) is released. Then, the desulfurized flue gas (DS-GAS) is emitted to the absorber for CO_2 capture [11,12]:

$$Mg^{2+} + SO_4^{2-} + 7H_2O \rightarrow MgSO_4{\cdot}7H_2O \tag{25}$$

$$Mg^{2+} + HSO_3^- + 3H_2O \rightarrow MgSO_3{\cdot}3H_2O + H^+ \tag{26}$$

$$Mg^{2+} + HSO_3^- + 6H_2O \rightarrow MgSO_3{\cdot}6H_2O + H^+ \tag{27}$$

The scrubber specifications are as follows: the temperature is set at 60 °C, and the pressure is set at 1 atm based on the results of the study by Lim et al. [22]. In SO_x capture, the $MgSO_3$ concentration in the liquid phase is critical. If the concentration of the $MgSO_3$ is less than the lower limit, SO_2 capture efficiency decreases. After a certain threshold, $MgSO_3$ starts to precipitate in the solution and there is a risk of scale formation. The total $MgSO_3$ concentration in the liquid phase is approximately 5–8 wt%, and in general, the proper concentration of the $MgSO_3$ is 1 wt%. Thus, another 4–7 wt% of $MgSO_3$ should be oxidized to $MgSO_4$ to maintain the $MgSO_3$ concentration. Therefore, to maintain the $MgSO_3$ concentration, oxidization air is allowed through the bottom of the scrubber. Thus, $MgSO_3$ is forcibly converted to $MgSO_4$.

2.3.4. CO_2 capture and utilization

Desulfurized flue gas is passed to the absorber (ABSORBER) for CO_2 capture. KOH generated from electrodialysis of the seawater bittern is used in the proposed process. KOH is inserted at the top of the absorber, and desulfurized flue gas is entered at the bottom of the absorber to maximize the gas–liquid contact surface reaction. Because of the gas–liquid contact surface reaction, CO_2 is converted to HCO_3^- and CO_3^{2-} according to the following processes [30]:

$$CO_2(g) \rightarrow CO_2(aq) \tag{28}$$

$$2KOH \rightarrow 2K^+ + 2OH^- \tag{29}$$

$$CO_2 + OH^- \leftrightarrow HCO_3^- \tag{30}$$

$$HCO_3^- + OH^- \leftrightarrow H_2O + CO_3^{2-} \tag{31}$$

$$2K^+ + CO_3^{2-} \rightarrow K_2CO_3 \tag{32}$$

To model the absorber, the rate-based Radfrac model was used. The total stage number was set to 20, and MELLAPAK SULZER 350Y column packing was used [31]. Furthermore, the total height of packing, inner diameter, and top pressure in the absorber were 3.89 m, 0.1 m, and 1.5 bar, respectively [32]. Finally, CO_2 captured flue gas (CLEANGAS) is emitted at the top of the absorber, and the rich solution (RICHOUT) with

Table 1
Conventional cases of SO_x and CO_2 capture and utilization.

Classification		Case	Process type	Process features
SCU	SO_x capture efficiency	S1	WFGD	Ca/S ratio = 1.50
		S2	WFGD	Ca/S ratio = 1.03
		S3	DFGD	Ca/S ratio = 2.00
		S4	DFGD	Ca/S ratio = 2.23
CCU	CO_2 capture efficiency	C1	CCS using amine	0.3 mol CO_2 loading/mol MEA
		C2	CCS using amine	0.2 mol CO_2 loading/mol MEA
		C3	CCS using NaOH	50 wt% NaOH
		C4	CCS using NaOH	L/G ratio = 4.30

Table 2
Simulation results of $KClO_4$ precipitation.

Components	SWB [mol/h]	HClO4 [mol/h]	KClO4 [mol/h]
H_2O	8147	77.59	8225
H^+	–	–	180.9
Na^+	54.46	–	54.46
K^+	181.1	–	0.150
Mg^{2+}	501.9	–	501.9
$HClO_4$	–	181.1	0.150
$KClO_4$	–	–	180.9
Total	8885	258.6	9144

abundant HCO^- and CO_3^{2-} is used in the $Mg(OH)_2$ carbonation process (MG-CARBO), which proceeds as follows [22]:

$$Mg^{2+} + CO_3^{2-} \leftrightarrow MgCO_3 \tag{33}$$

$$Mg^{2+} + HCO_3^- \leftrightarrow MgCO_3 + H^+ \tag{34}$$

To model the $Mg(OH)_2$ carbonation process, the RCSTR model is used and the equilibrium constants of the aforementioned reaction is considered based on Gibbs free energy minimization.

3. Results and discussion

This section presents the simulation results of the proposed process involving metal ion separation, SCU, and CCU. Next, to investigate SO_x and CO_2 capture efficiency, eight conventional cases were set, and the SO_x and CO_2 capture efficiency of the proposed process was compared to each conventional case. To capture the SO_x, the conventional cases were classified into wet flue gas desulfurization (WFGD) and dry flue gas desulfurization (DFGD). Each desulfurization method had a different Ca/S ratio, which is the main parameter determining the SO_x capture efficiency. To capture the CO_2, the conventional cases were classified into carbon capture storage (CCS) using amine and CCS using NaOH. Next, the economic feasibility of the suggested process is investigated by calculating the pay-back period (PBP) in economic assessment. Table 1 presents the conventional cases of SO_x and CO_2 capture and utilization.

3.1. Simulation results

3.1.1. Metal ion separation results

K^+ ions were converted to $KClO_4$ following the reaction with $HClO_4$ based on the difference of the solubility. Because $HClO_4$ is expensive, $HClO_4$ of approximately 181 mol/h is added, which results in the same amount of K^+ ions. Table 2 presents the simulation results of $KClO_4$ precipitation.

As seen in Table 2, approximately 181.1 mol/h of $HClO_4$ reacts with 181.1 mol/h of K^+ ions, and 180.9 mol/h of $KClO_4$ is generated, which indicates a conversion rate of 99.92 %. The results indicate that most of K^+ ions react with $HClO_4$ and are precipitated. $KClO_4$, which exhibits the lowest solubility at 25 °C out of all the alkali metal perchlorates, is precipitated based on the solubility difference of the perchlorate and each metal ion. $KClO_4$ is precipitated first because the solubility of $Mg(ClO_4)_2$, which is generated when $HClO_4$ is added to seawater bittern, is significantly greater than that of $KClO_4$. The solubility of $KClO_4$ in water is 1.5 g/100 mL, that of $Mg(ClO_4)_2$ is 99.3 g/100 mL, and that of $Na(ClO_4)_2$ is 209.6 g/100 mL. The precipitation rate of $KClO_4$ is determined using the temperature and pH level. In this study, the temperature and the pH level are set as −7 °C and 2, respectively, based on a study performed by Chen et al. [24]. Next, the generated $KClO_4$ is added to the decomposition process. The decomposed $KClO_4$ is converted to KOH in the electrolysis process. Table 3 presents the simulation results of the K^+ ion separation.

Table 3
Simulation results of K^+ ion separation.

Components	KClO4-S [mol/h]	KCl + O2 [mol/h]	KOH [mol/h]
H_2O	–	–	74,820
OH^-	–	–	180
K^+	–	–	180
$KClO_4$	180.9	0.9	–
KCl	–	180	–
O_2	–	360	–
H_2	–	–	90
Cl_2	–	–	90
Total	180.9	540.9	75,360

Table 4
Simulation results of Mg^{2+} ion separation.

Components	MG-CONC [mol/h]	NAOH [mol/h]	MGOH2 [mol/h]
H_2O	8225	1355	9580
H^+	180.9	–	180.9
OH^-	–	1355	351.4
Na^+	54.46	1355	1410
K^+	0.15	–	0.15
Mg^{2+}	501.9	–	–
$Mg(OH)_2$	–	–	501.9
Total	8962	4066	12,024

Table 5
Simulation results of SO_x capture and utilization.

Components	MG-ION1 [mol/h]	FLUEGAS [mol/h]	DESULF [mol/h]
H_2O	1.094	17.28	17.97
Mg^{2+}	0.652	–	0.652
SO_2	–	0.403	–
HSO_3^-	–	–	1.915×10^{-10}
SO_4^{2-}	–	–	0.403
O_2	–	95.04	94.84
N_2	–	374.4	374.4
CO_2	–	89.28	89.28
HSO_3^-, SO_4^{2-} → $MgSO_4 \cdot 7H_2O$ 99.9 % conversion rate			

As seen in Table 3, approximately 180.9 mol/h of $KClO_4$ is decomposed and converted to 180 mol/h of KCl. Next, KCl is electrolyzed, and 180 mol/h of K^+ and OH^- ion are generated with a conversion rate of 99.5 %. Table 4 presents the simulation results of Mg^{2+} ion separation.

According to the table, approximately 501.9 mol/h of Mg^{2+} ions in seawater bittern react 1355 mol/h of NaOH to generate 501.9 mol/h of $Mg(OH)_2$, which indicates a conversion rate of 99.9 %. In addition to $Mg(OH)_2$, minerals such as NaCl and $Na_2SO_4 \cdot 10H_2O$ may also be precipitated. However, most of these materials can be removed by washing with water because their solubility in water is high. Therefore, the produced $Mg(OH)_2$ exhibits a high purity of approximately 94 %. The additional $Mg(OH)_2$ remaining after the desulfurization and $Mg(OH)_2$ carbonation processes can be commercialized as an antacid and emollient for additional economic benefit.

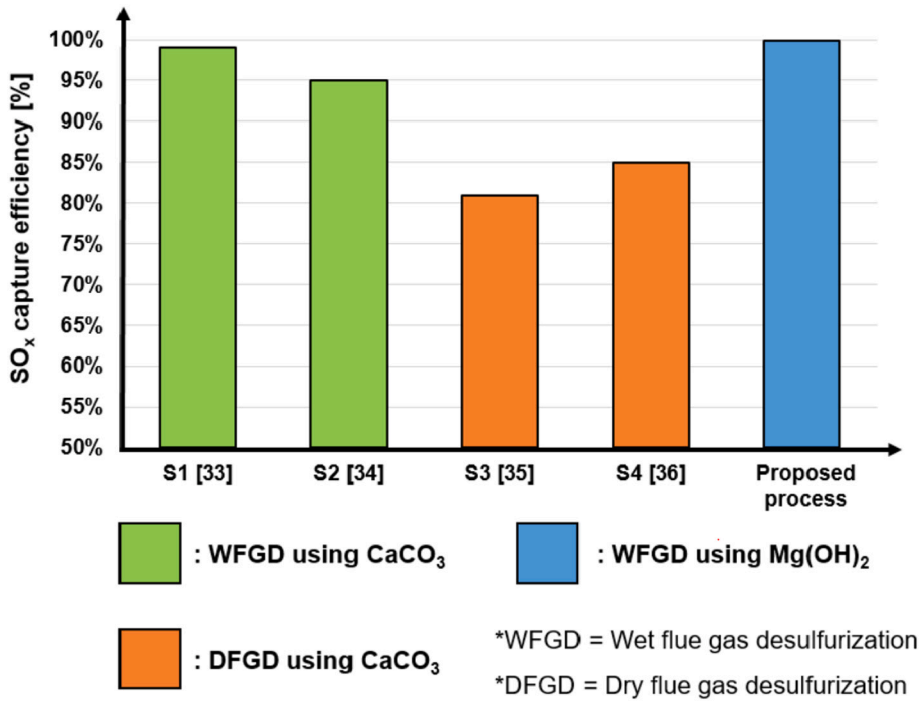

Fig. 4. SO_x capture efficiency of the proposed and conventional processes.

3.1.2. SOx capture and utilization results

For SO_x capture and utilization, $Mg(OH)_2$ through precipitation and acidification processes is used as the SO_x absorbent. Subsequently, split $Mg(OH)_2$ dissolved with water is sprayed at the top of the scrubber. During the vapor–liquid contact with alkaline slurry and flue gas, SO_x is captured. Table 5 displays the simulation results of SCU.

As seen in Tables 5, 0.403 mol/h of SO_x is converted to 0.403 mol/h of SO_4^{2-} on reacting with 0.652 mol/h of Mg^{2+}. Therefore, the SO_x capture efficiency is determined to be 99.9 %, and the conversion rate of $MgSO_4{\cdot}7H_2O$ from HSO_3^- and SO_4^{2-} is approximately 99.9 %. When SO_x is captured, HSO_3^- and SO_4^{2-} are generated and the conversion rate of aforementioned substances is determined according to the pH level of the liquid phase. Because in the proposed process, $Mg(OH)_2$, which indicates alkaline; thus, SO_4^{2-} is abundant because of the high pH level. Although SO_2 is also converted to HSO_3^-, the amount is very small, and limited $MgSO_3{\cdot}3H_2O$ and $MgSO_3{\cdot}6H_2O$, which are formed by the reaction of Mg^{2+} ions and HSO_3^- ions, were produced. Most of the converted SO_4^{2-} ions reacted with Mg^{2+} ions at the bottom of the scrubber to produce epsom salt, which exhibits a wide application in textile, tanning, and agricultural industry. Next, Fig. 4 details SO_x capture efficiency of the proposed and conventional process.

SO_x capture and utilization is generally classified into dry flue gas desulfurization (DFGD) and wet flue gas FGD (WFGD) as the moisture content of the SO_x absorbent. In both the desulfurization process, Ca-based SO_x absorbents are generally used and limestone ($CaCO_3$) and lime (CaO) are representative SO_x absorbents because of their low cost.

Table 6
Simulation results of CO_2 capture and utilization.

Components	DS-GAS [mol/h]	CLEANGAS [mol/h]	RICHOUT [mol/h]
H_2O	15.15	15.69	74,820
CO_2	89.28	1.782	6.451×10^{-6}
HCO_3^-	–	–	1.793
CO_3^{2-}	–	–	85.70
O_2	94.84	94.52	0.314
N_2	374.4	373.8	0.628
$Mg^{2+} + HCO_3^-, CO_3^{2-} \rightarrow MgCO_3$ 90.03 % conversion rate			

From the analysis of many desulfurization absorbents, it was observed that the commercialized desulfurization technologies, such as DFGD and WFGD, used a Ca-based absorbent; thus, the proposed model focused only on this concept.

As seen in Fig. 4, the SO_x capture efficiency of cases S1 and S2 (WFGD) were approximately 99.0 % and 95.0 %, respectively [33,34]. Next, the SO_x capture efficiency of cases B1 and B2 (DFGD) was 81.0 % and 85.0 %, respectively [35,36]. The results revealed that DFGD exhibited a lower efficiency compared with WFGD. Therefore, WFGD exhibits a higher desulfurization efficiency because WFGD exhibits a longer reaction time than that exhibited by DFGD; thus, the removal efficiency of SO_x is high, and the generation of unreacted absorbent is low. In addition, because the desulfurization of WFGD corresponds to the liquid–vapor contact, the reaction rate of WFGD was higher than that of DFGD. The SO_x capture efficiency of the proposed process, in which $Mg(OH)_2$ is used as the SO_x absorbent, was 99.9 %. Because $Mg(OH)_2$ is a stronger base than $CaCO_3$, the SO_x capture efficiency of $Mg(OH)_2$ can be increased. The proposed process can increase the SO_x capture efficiency by 0–4 % and 15–19 % compared with conventional WFGD and DFGD, respectively.

In conventional SCU, $CaCO_3$ typically obtained from limestone is used as the SO_x absorbent. Because other substances, such as SiO_2 and Al_2O_3 decrease the purity of desulfurization gypsum, which is a by-product of SCU, limestone purity of $CaCO_3$ should be more than 94 wt % (i.e., high-grade limestone). However, high-grade limestone reserves are only 20 % of the total reserves. Therefore, a substitute for high-grade limestone is required. Furthermore, in SCU using $CaCO_3$, CO_2 is emitted for SO_x removal; thus, increased greenhouse gas emission may occur. The conventional desulfurization method is not feasible because after a certain limit, instead of the CCU process, CO_2 is generated. Lime (CaO) is also used as an SO_x absorbent and does not emit CO_2; however, $CaCO_3$ sintering is required at high temperatures, which causes additional combustion of fossil fuels and increases the cost.

However, in the proposed process, because seawater bittern substitutes high-grade limestone, resource depletion is mitigated. Furthermore, the cost for mining the limestone is reduced, and the generated $MgSO_4{\cdot}7H_2O$ can be sold. $Mg(OH)_2$ generated from the metal ions in

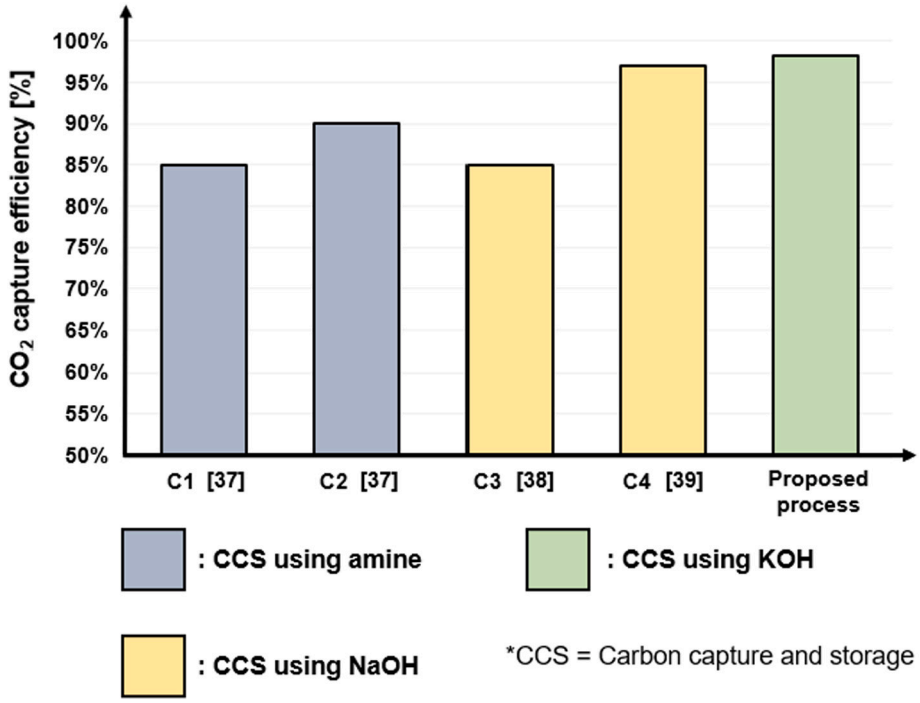

Fig. 5. CO_2 capture efficiency of the proposed and conventional processes.

seawater bittern is used in the SCU system. Thus, a carbon-neutral desulfurization method was realized. Thus, additional CO_2 generation is not a concern.

3.1.3. *CO_2 capture and utilization results*

To capture CO_2 in flue gas, KOH is used as a CO_2 absorbent that is generated in the metal ion separation procedure. During the vapor–liquid contact with KOH and desulfurized flue gas at the absorber, CO_2 is captured. Next, the captured CO_2 exists in ionic rich flow, which contains HCO_3^- and CO_3^{2-}, and the rich flow reacts with Mg^{2+} ions at the $Mg(OH)_2$ carbonation process to generate $MgCO_3$. Table 6 displays the simulation results of CCU.

As seen in Table 6, 89.28 mol/h of CO_2 in DS-GAS is entered in an absorber, and 98 % of CO_2 is captured. The captured CO_2 was emitted in the form of CO_3^{2-} and HCO_3^-, and the proportion of CO_3^{2-} and HCO_3^- varied depending on the pH. CO_2 is mainly in the form of CO_3^{2-} based on the acid-base equilibrium. As a result of carbonation, 90.03 % of Mg^{2+} was converted to $MgCO_3$. Fig. 5 reveals the CO_2 capture efficiency of the proposed and conventional processes.

As seen in Fig. 5, the CO_2 capture efficiencies of cases C1 and C2,

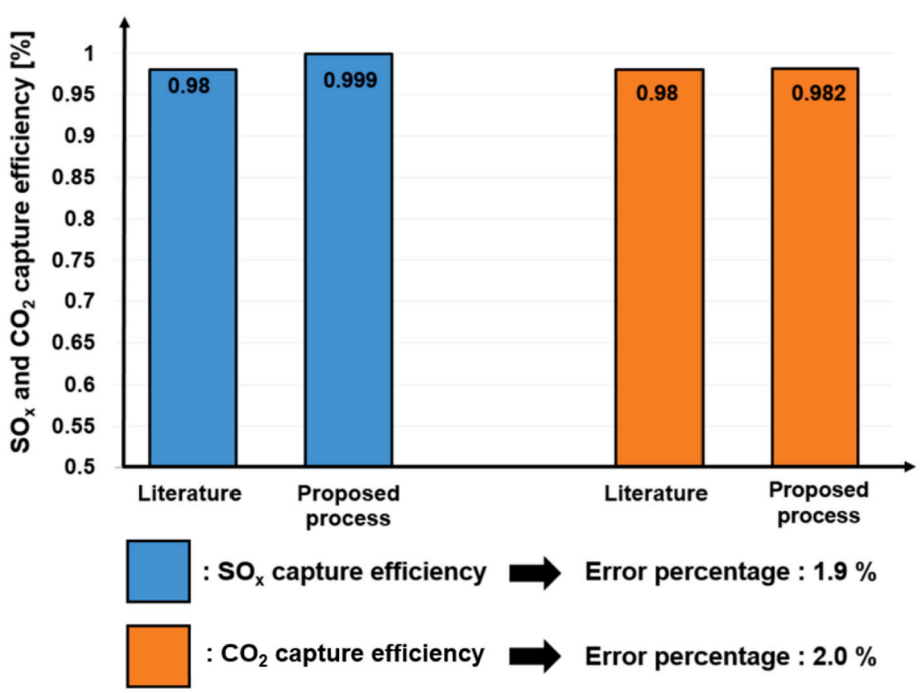

Fig. 6. Validation results of proposed process.

wherein amine is used as the CO_2 absorbent, were 85.0 % and 90.0 %, respectively [37], and those of cases C3 and C4, wherein NaOH solution is used as the CO_2 absorbent, were 85.0 % and 97.0 %, respectively [38,39]. By contrast, the proposed process captured 98.2 % of CO_2, which indicates the highest CO_2 capture efficiency. Amines such as mono-ethanolamine (MEA) or NaOH are used as CO_2 absorbents. First, the amine exhibits high reactivity with CO_2 and low cost. However, the amine solution exhibits low CO_2 absorption capacity, and if the solution reacts with other acid components, such as formic acid and acetic acid, heat-stable salt is produced, which causes considerable losses of the absorbent during CO_2 capture and results in low CO_2 capture efficiency [40]. Second, NaOH cannot be reused; thus, raw material cost and feedstock availability increases considerably. When the CO_2 absorption rate reaches limited concentration, NaOH emits CO_2 rather than absorbing it. Because CO_2 is captured using NaOH, NaOH is converted to $NaHCO_3$ and based on the phase equilibrium, CO_2 is reemitted from $NaHCO_3$. Thus, a limit to CO_2 isolation exists as a metal salt using the NaOH solution. By contrast, KOH exhibited uniform absorption of CO_2 with limited concentration. When KOH reacts with CO_2, it is neutralized according to the zwitterion mechanism. Thus, KOH continuously absorbs CO_2 by the counter action of K^+ ions, including direct absorption and conversion. Thus, KOH exhibits strong CO_2 binding affinity and effective CO_2 capture from ambient air. However, the use of KOH is limited by high cost and low production rate [41]. In the proposed process, KOH is generated by separating metal cations in seawater bittern. Therefore, in the proposed process, KOH is used without any feedstock limitation for solving the conventional CCS process. Thus, the process is economically feasible.

3.1.4. Model validation

Fig. 6 shows the validation results of proposed process. A comparative process that uses the same absorbents as the used in the proposed model was employed to validate the simulation results of the proposed model, and the capture efficiencies of SO_x and CO_2 were compared. The SO_x capture efficiency of the suggested process was approximately 99.9 % and that of the comparative process, which uses $Mg(OH)_2$, was approximately 98 % [28]. Therefore, the error percentage of the suggested process was approximately 2.0 %, which indicates a high accuracy. Furthermore, to validate the CO_2 capture efficiency, the comparative process, which uses KOH, was employed, and it was observed that the CO_2 capture efficiency of the comparative process was 98.0 % [42]. Therefore, because the CO_2 capture efficiency of the proposed model was approximately 98.2 %, the error percentage was determined to be 2.0 %. Using these parameters, the feasibility of the model proposed in this study was confirmed.

3.2. Economic assessment

An economic assessment was conducted to preliminarily detail the economic feasibility of the proposed process. The pay-back period (PBP) for additional equipment installation was calculated. The economic feasibility of the proposed process was investigated by comparing with the conventional process. PBP was determined from the increase fixed capital investment (FCI), which is calculated by subtracting FCI of the conventional process from the FCI of the proposed process.

3.2.1. Pay-back period

The PBP indicates the time required to recover the cost of an additional investment, and it is calculated by dividing the increased FCI (*Increased FCI*) by net annual revenue (*Net annual revenue*) as follows [43]:

$$PBP = \frac{Increased\ FCI}{Net\ annual\ revenue} \tag{35}$$

The FCI is the fixed cost for process design and equipment construction and installation. FCI calculated by summing direct cost (C^{direct}) and indirect cost ($C^{indirect}$) as follows [45,46]:

$$FCI = C^{direct} + C^{indirect} \tag{36}$$

In FCI calculation, first C^{direct} is determined by summing inside battery limit cost (C^{ISBL}) and the outside battery limit cost (C^{OSBL}) as follows [46]:

$$C^{direct} = C^{ISBL} + C^{OSBL} \tag{37}$$

Here, C^{ISBL} is calculated by summing equipment cost ($C^{equipment}$), installation cost ($C^{installation}$), control cost ($C^{control}$), piping cost (C^{piping}), and electrical cost ($C^{electrical}$) as follows [47]:

$$C^{ISBL} = C^{equipment} + C^{installation} + C^{control} + C^{piping} + C^{electrical} \tag{38}$$

where $C^{equipment}$ is composed of equipment cost of the electrolysis process, acidification process, precipitation, and decomposition process and is determined based on six-tenth rule as follows [48]:

$$C^{equipment} = \frac{CEPCI^{2022}}{CEPCI^{Referenced\ year}} \times REC \times \left(\frac{PC}{RC}\right)^{0.6} \tag{39}$$

where $CEPCI^{2022}$ denotes the chemical plant cost indexes at 2022, $CEPCI^{Referenced\ year}$ denotes chemical plant cost indexes at the referenced year, *REC* denotes the referenced equipment cost, *PC* denotes the capacity of the proposed process, and *RC* denotes referenced capacity. To evaluate the equipment costs of the various processes, the Aspen plus Economic Analyzer, which is a cost-estimating software that evaluates the capital and operating cost, is used. However, the equipment cost of it is analyzed based on the method used by Herz et al. because the electrolysis process is modeled using MATLAB® version R2020b [49].

Here, $C^{installation}$ and C^{piping} are estimated 10 % of the FCI as follows [50]:

$$C^{installation} = C^{piping} = 0.1 \times FCI \tag{40}$$

Here, $C^{control}$ and $C^{electrical}$ is determined to be 5 % of the FCI as follows [50]:

$$C^{control} = C^{electrical} = 0.05 \times FCI \tag{41}$$

Here, C^{OSBL} is determined from the building cost ($C^{building}$), site preparation cost ($C^{site\ preparation}$), services facility cost ($C^{services\ facility}$), and land cost (C^{land}) as follows [50]:

$$C^{OSBL} = C^{building} + C^{site\ preparation} + C^{services\ facility} + C^{land} \tag{42}$$

Here, $C^{building}$ and $C^{services\ facility}$ is determined 8 % of FCI as follows [50]:

$$C^{building} = C^{services\ facility} = 0.08 \times FCI \tag{43}$$

Furthermore, $C^{site\ preparation}$ and C^{land} are estimated 2 % of the FCI as follows [50]:

$$C^{site\ preparation} = C^{land} = 0.02 \times FCI \tag{44}$$

In FCI calculation, $C^{indirect}$ is determined by summing engineering ($C^{engineering}$), construction ($C^{construction}$), contractor ($C^{contractor}$), and contingency costs ($C^{contingency}$), and all the costs are estimated 5 % of FCI as follows [51]:

$$C^{indirect} = C^{engineering} + C^{construction} + C^{contractor} + C^{contingency} \tag{45}$$

$$C^{engineering} = C^{construction} = C^{contractor} = C^{contingency} = 0.05 \times FCI \tag{46}$$

Next, *Net annual revenue* is determined from the profit according to sales $MgCO_3$, $MgSO_4{\cdot}7H_2O$, and residual $Mg(OH)_2$, which remains after SO_x capture, thus, saving KOH and $Mg(OH)_2$ absorbent and reducing the cost of $HClO_4$ and HCl. *Net annual revenue* is calculated by subtracting the sum of the revenue of the sales product ($R^{product}$) and revenue of saving absorbent ($R^{absorbent}$) from the raw material cost ($C^{raw\ material}$) as follows:

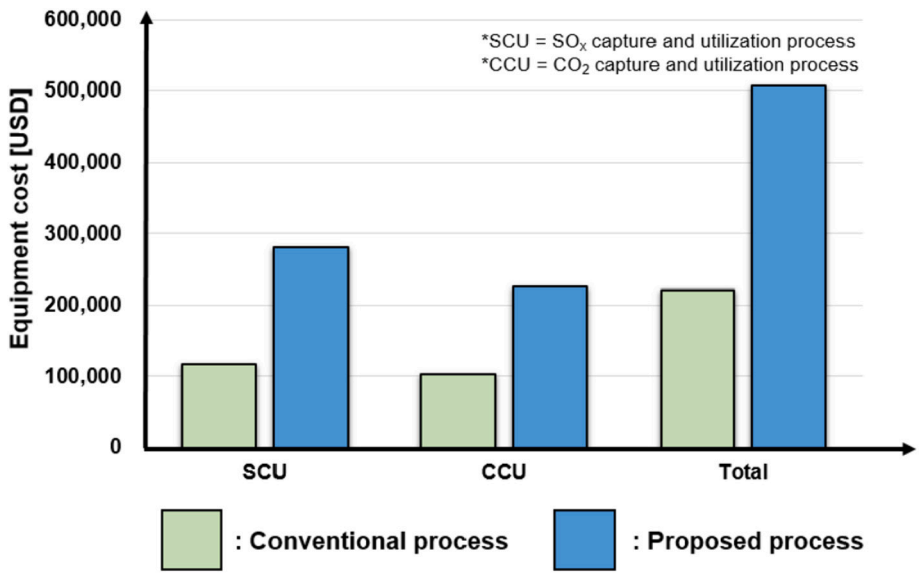

Fig. 7. Equipment costs of the conventional and proposed processes.

Table 7
FCI of the proposed process.

Classification	Description	Cost [USD]
$C^{equipment}$	Additional equipment cost	285,365
$C^{installation}$	Installation cost	95,122
$C^{control}$	Control cost	47,561
C^{piping}	Piping cost	95,122
$C^{electrical}$	Electrical cost	47,561
$\boldsymbol{C^{ISBL}}$	**Inside battery limit cost**	**570,731**
$C^{building}$	Building cost	76,097
$C^{site\ preparation}$	Site preparation cost	19,024
$C^{service\ facilities}$	Service facilities cost	76,097
C^{land}	Land cost	19,024
$\boldsymbol{C^{OSBL}}$	**Onside battery limit cost**	**190,242**
$\boldsymbol{C^{direct}}$	**Direct cost**	**760,973**
$C^{engineering}$	Engineering cost	47,561
$C^{construction}$	Construction cost	47,561
$C^{contractor}$	Contractor cost	47,561
$C^{contingency}$	Contingency cost	47,561
$\boldsymbol{C^{indirect}}$	**Indirect cost**	**190,244**
FCI	**Fixed capital investment**	**951,217**

Table 8
Annual revenue of the products generated in the proposed process [1,50].

Classification	Price [USD/ton]	Production [ton/y]	Profit [USD/y]
$Mg(OH)_2$	400	223.25	89,300
$MgCO_3$	700	42.98	30,086
$MgSO_4{\cdot}7H_2O$	185	0.87	161
$R^{product}$	–	–	119,547

$$Net\ annual\ revenue = R^{product} + R^{absorbent} - C^{raw\ material} \tag{47}$$

3.2.2. Economic assessment results

First, Fig. 7 details the equipment cost of the conventional and proposed processes. From the Fig. 7, in the conventional process, the equipment cost of the SCU [52] and CCU [53] is USD 117,865 and USD 103,800, respectively. Thus, the total equipment cost of the conventional process is USD 221,665. By contrast, the equipment cost of the SCU and CCU of the proposed process is USD 280,917 and 226,113, respectively, and the total equipment cost of the proposed process is USD 507,030, which indicates an increase of 228 % compared to equipment cost of conventional case. Because additional equipment is required for processes, such as the electrolysis, acidification, precipitation, and decomposition processes, the total equipment cost of the proposed process is increased by approximately USD 285,365. Then, based on the determined increased equipment cost, FCI is calculated and Table 7 details the FCI of the proposed process.

Table 9
Annual cost of the absorbent consumed in the conventional process [51].

Classification	Price [USD/ton]	Saving [ton/y]	Profit [USD/y]
KOH	1350	88.53	119,516
$Mg(OH)_2$	400	0.42	168
$R^{absorbent}$	–	–	119,684

Table 10
Annual raw material costs of the proposed process [56].

Classification	Price [USD/ton]	Consumption [ton/y]	Cost [USD/y]
$HClO_4$	528	159.4	84,163
HCl	30	54.3	1629
$[C^{raw\ material}$	–	–	85,792

As seen in Table 7, the C^{ISBL} is USD 570,731, C^{OSBL} is calculated to be USD 190,242, and the C^{direct} and $C^{indirect}$ are USD 760,973 and USD 190,244, respectively. Thus, the FCI is finally determined to be USD 951,217.

Net annual revenue is calculated by subtracting the sum of $R^{product}$ and $R^{absorbent}$ from $C^{raw\ material}$. Table 8 details the annual revenue of the product generated in the proposed process.

As seen in Table 8, 223.25 ton/y of the residual $Mg(OH)_2$ generated a profit of approximately 89,300 USD/y and 42.98 ton/y of the $MgCO_3$ generated a profit approximately 30,086 USD/y. The 161 USD/y of profit is generated from the 0.87 ton/y of the $MgSO_4{\cdot}7H_2O$. Thus, the $R^{product}$ is finally determined to be 119,547 USD/y. Table 9 details the annual revenue of the saving absorbent.

As seen in Table 9, a profit of 119,516 USD/y is obtained from the 88.53 ton/y of KOH savings. Because 0.42 ton/y of Mg(OH)2 is saved, 168 USD/y of profit is generated. Finally, the $R^{absorbent}$ is determined to be 119,684 USD/y. Table 10 shows the annual raw material cost of the proposed process.

As seen in Table 10, 84,163 USD/y of cost is consumed as 159.4 ton/y of HClO4 is consumed for the $KClO_4$ precipitation process. Here, 1629 USD/y of cost because 54.3 ton/y of HCl is consumed for the

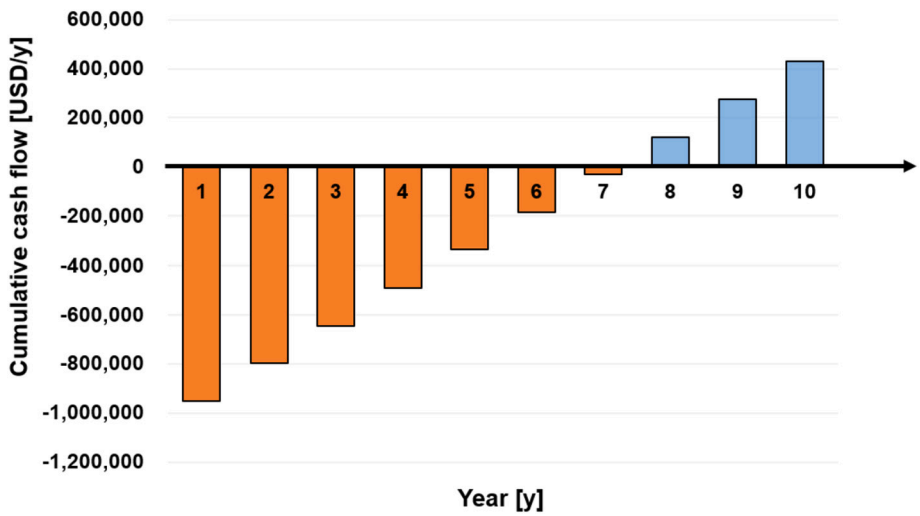

Fig. 8. Cumulative cash flow of the proposed process.

acidification process. Thus, $C^{raw\ material}$ is determined to be 85,792 USD/y. *Net annual revenue* is finally determined by 153,439 USD/y from the calculated $R^{product}$, $R^{absorbent}$, and $C^{raw\ material}$. Fig. 8 displays the cumulative cash flow of the proposed process.

From the Fig. 8, the cumulative cash flow at 1 y is approximately −951,517 USD/y according to increased FCI. The cumulative cash flow has negative value until 6 y and in 7 y, the cumulative cash flow is determined to be 122,556 USD/y. Next, after 7 y, the cumulative cash flow increases considerably. The determined PBP is 6.2 y and after 6.2 y, 153,439 USD/y of additional profit can be obtained. Despite the increase in FCI as installation of the additional equipment such as electrolysis, acidification, precipitation. and decomposition processes, the proposed process has the following economic advantages: (1) the proposed process can save the purchasing cost of the absorbent for CO_2 and SO_x capture by using valuable metal ions in seawater bittern; (2) the proposed process can capture CO_2 and SO_x as well as use $MgCO_3$, $MgSO_4{\cdot}7H_2O$, and residual $Mg(OH)_2$, which remain after SO_x capture and these products earn profits through sales. The capacity of the proposed process is small. However, if its capacity was large, the cost savings associated with the raw materials and the revenue from the products would increase linearly. As the increase in the equipment cost, through the installation of additional equipment, gradually decreases with an increase in the capacity, the economic feasibility is of the proposed process is expected to be superior.

In this study, an economic evaluation was conducted based on the simulation results and the equipment costs of the proposed model in order to evaluate the economic feasibility of the proposed process. However, for field applications, it is necessary to consider major parameters such as installation cost, control cost, and electrical cost rigorously rather than estimating them as ratios.

4. Conclusion

In this study, a novel seawater bittern recovery process for CO_2 and SO_x utilization was proposed. This study made two major contributions to existing literature. First, because in the proposed novel process, metal ions in seawater bittern are used for CCU and SCU, the process is an appropriate solution to mitigate environmental contamination using waste seawater bittern and feedstock restrictions of the conventional absorbents. Second, this study proposed an environmental and economical approach to capture and utilize CO_2 and SO_x in the flue gas emitted from the power plant using only seawater bittern that is otherwise generally discharged. Therefore, since seawater is easily available, the proposed method is efficient and environmentally friendly. SO_x capture efficiency of the proposed method is 99 % and CO_2 capture efficiency is 98.0 %. Furthermore, the annual profit can be increased by 153,439 USD/y. The PBP is determined to be 6.2 y; thus, the method is profitable and suitable for large-capacity processes. This study provides considerable insights into the efficient use of seawater bittern and cost-effective and environmentally friendly SO_x and CO_2 capture and utilization.

This work focuses on the conceptual design of the SO_2 and CO_2 capture and utilization processes using seawater bittern. However, the main parameters that determine the capture efficiency of SO_2 and CO_2, such as mean residence time of flue gas, surface area of the absorbent, and liquid-gas ratio, will be determined optimally in further studies.

CRediT authorship contribution statement

- Jonghun Lim: Writing - Original Draft, Formal analysis
- Deok Ju Kim: Conceptualization, Methodology
- Hyungtae Cho: Investigation, Methodology
- Junghwan Kim: Writing - Review & Editing, Project administration

Declaration of competing interest

The authors declare that they have no known competing financial interests or personal relationships that could have appeared to influence the work reported in this paper.

Acknowledgement

This work was supported by the Korean Institute of Industrial Technology within the framework of the following projects: “Development of Global Optimization System for Energy Process [grant number IR-22-0040, IZ-22-0049, UR-22-0031]”, “Development of complex parameter smart analysis modules for color customering [grant number EH-22-0011]” and “Development of AI Platform for Continuous Manufacturing of Chemical Process [grant number JH-22-0004]”.

Appendix A. Supplementary data

Supplementary data to this article can be found online at https://doi.org/10.1016/j.desal.2022.115995.

References

[1] S. Cho, J. Lim, H. Cho, Y. Yoo, D. Kang, J. Kim, Novel process design of desalination wastewater recovery for CO2 and SOX utilization, Chem. Eng. J. (2021), 133602, https://doi.org/10.1016/j.cej.2021.133602.

[2] Heru Susanto, Nur Rokhati, G.W. Santosa, Development of traditional salt production process for improving product quantity and quality in Jepara District, Central Java, Indonesia, Procedia Environ. Sci. 23 (2015) 175–178, https://doi.org/10.1016/j.proenv.2015.01.027.

[3] T. Kuda, T. Yano, Mineral composition of seawater bittern nigari products and their effects on changing of browning and antioxidant activity in the glucose/lysine maillard reaction, Appl. Biochem. Biotechnol. 172 (2014) 2989–2997, https://doi.org/10.1007/s12010-013-0722-0.

[4] C.K. Na, H. Park, Recycling of waste bittern from salt farm (I): recovery of magnesium, Appl. Chem. Eng. 27 (2016) 427–432, https://doi.org/10.14478/ace.2016.1058.

[5] W. Song, Z. Li, F. Liu, Y. Ding, P. Qi, H. You, C. Jin, Effective removal of ammonia nitrogen from waste seawater using crystal seed enhanced struvite precipitation technology with response surface methodology for process optimization, Environ. Sci. Pollut. Res. 25 (2018) 628–638, https://doi.org/10.1007/s11356-017-0441-0.

[6] A. Chandra, P. Malik, S. Singh, A. Roy, N. Sahoo, M. Singh, Sustainable research methodology for potassium nitrate recovery from seawater, Chem. Eng. Process. - Process Intensif. 174 (2022), 108870, https://doi.org/10.1016/j.cep.2022.108870.

[7] F.W. Jumaeri, E.F. Mahatmanti, D. Rahayu, A.N.K. Qoyyima, Ningrum, recovery of high purity sodium chloride from seawater bittern by precipitation-evaporation method, J. Phys. Conf. Ser. 1918 (2021), https://doi.org/10.1088/1742-6596/1918/3/032023.

[8] H. Amrulloh, Y.S. Kurniawan, C. Ichsan, J. Jelita, W. Simanjuntak, R.T. M. Situmeang, P.A. Krisbiantoro, Highly efficient removal of Pb(II) and Cd(II) ions using magnesium hydroxide nanostructure prepared from seawater bittern by electrochemical method, Colloids Surf. A Physicochem. Eng. Asp. 631 (2021), 127687, https://doi.org/10.1016/j.colsurfa.2021.127687.

[9] V.S. Nalajala, N.J. Kothamasu, R.N. Mandapati, R.V.S.N. Chaganti, T. Subbaiah, Preparation of magnesium chloride from sea water bitterns using techniques of spray and thermal drying, J. Mater. Eng. Perform. (2022) 1–6, https://doi.org/10.1007/s11665-022-06841-1.

[10] P. Sahu, S.C. Upadhyay, S. Bhatti, J.K. Mahey, R.J. Sanghavi, A. Kumar, Sodium-sulphate production from sulphate-rich bittern: a parametric study and economic evaluation, J. Environ. Chem. Eng. 9 (2021), 105632, https://doi.org/10.1016/j.jece.2021.105632.

[11] C.-K. Na, H. Park, E.H. Jho, Utilization of waste bittern from saltern as a source for magnesium and an absorbent for carbon dioxide capture, Environ. Sci. Pollut. Res. 24 (2017) 1–10, https://doi.org/10.1007/s11356-017-9913-5.

[12] J. Lim, Y. Choi, G. Kim, J. Kim, Modeling of the wet flue gas desulfurization system to utilize low-grade limestone, Korean J. Chem. Eng. 37 (2020) 2085–2093, https://doi.org/10.1007/s11814-020-0639-6.

[13] J. Lim, J. Kim, Optimization of a wet flue gas desulfurization system considering low-grade limestone and waste oyster Shell, J. Korea Soc. Waste Manag. 37 (2020) 263–274, https://doi.org/10.9786/kswm.2020.37.4.263.

[14] J. Lim, H. Cho, J. Kim, Optimization of wet flue gas desulfurization system using recycled waste oyster shell as high-grade limestone substitutes, J. Clean. Prod. 318 (2021), 128492, https://doi.org/10.1016/j.jclepro.2021.128492.

[15] J. Lim, S. Jeong, J. Kim, Deep neural network-based optimal selection and blending ratio of waste seashells as an alternative to high-grade limestone depletion for SOX capture and utilization, Chem. Eng. J. (2021), 133244, https://doi.org/10.1016/j.cej.2021.133244.

[16] M. Yoo, S.J. Han, J.H. Wee, Carbon dioxide capture capacity of sodium hydroxide aqueous solution, J. Environ. Manag. 114 (2013) 512–519, https://doi.org/10.1016/j.jenvman.2012.10.061.

[17] A.V. Rayer, K.Z. Sumon, A. Henni, P. Tontiwachwuthikul, Kinetics of the reaction of carbon dioxide (CO2) with cyclic amines using the stopped-flow technique, Energy Procedia 4 (2011) 140–147, https://doi.org/10.1016/j.egypro.2011.01.034.

[20] J. Repke, Dynamic modeling and operation of the chlor-alkali process, Czas. Tech. 2016 (2016) 53–65, https://doi.org/10.4467/2353737XCT.16.006.4970.

[21] N. Meunier, S. Laribi, L. Dubois, D. Thomas, G. De Weireld, CO2 capture in cement production and re-use: first step for the optimization of the overall process, Energy Procedia 63 (2014) 6492–6503, https://doi.org/10.1016/j.egypro.2014.11.685.

[22] S. Cho, J. Lim, H. Cho, Y. Yoo, D. Kang, J. Kim, Novel process design of desalination wastewater recovery for CO2 and SOX utilization, Chem. Eng. J. 433 (2022), 133602.

[23] K.-H. Shin, A. Son, D.K. Cha, K.-W. Kim, Review on risks of perchlorate and treatment technologies, J. Korean Soc. Environ. Eng. 29 (2007) 1060–1068.

[24] W.S. Chen, C.H. Lee, Y.F. Chung, K.W. Tien, Y.J. Chen, Y.A. Chen, Recovery of rubidium and cesium resources from brine of desalination through t-BAMBP extraction, Metals (Basel) 10 (2020), https://doi.org/10.3390/met10050607.

[25] F.Y. Al-Aboosi, M.M. El-Halwagi, A stochastic optimization approach to the design of shale gas/oilwastewater treatment systems with multiple energy sources under uncertainty, Sustainability 11 (2019), https://doi.org/10.3390/su11184865.

[26] K. Thummar, R. Abang, K. Menzel, M.T. De Groot, Coupling a chlor-alkali membrane electrolyzer cell to a wind energy source: dynamic modeling and simulations, Energies 15 (2022), https://doi.org/10.3390/en15020606.

[27] B. Dou, W. Pan, Q. Jin, W. Wang, Y. Li, Prediction of SO2 removal efficiency for wet flue gas desulfurization, Energy Convers. Manag. 50 (2009) 2547–2553, https://doi.org/10.1016/j.enconman.2009.06.012.

[28] E. Salehi, B. Eidi, Z. Soleimani, An integrated process consisting of Mg(OH)2 –impregnated ceramic foam filters as adsorbent and Mg(OH)2 as scrubbing solution for intensified desulfurization of flue gas, Sep. Purif. Technol. 216 (2019) 34–42, https://doi.org/10.1016/j.seppur.2019.01.072.

[30] S. Hasan, A.J. Abbas, G.G. Nasr, Improving the carbon capture efficiency for gas power plants through amine-based absorbents, Sustainability 13 (2021) 1–28, https://doi.org/10.3390/su13010072.

[31] L.S. Tan, A.M. Shariff, K.K. Lau, M.A. Bustam, Factors affecting CO 2 absorption efficiency in packed column: a review, J. Ind. Eng. Chem. 18 (2012) 1874–1883, https://doi.org/10.1016/j.jiec.2012.05.013.

[32] M. Garcia, H.K. Knuutila, S. Gu, ASPEN PLUS simulation model for CO2 removal with MEA: validation of desorption model with experimental data, J. Environ. Chem. Eng. 5 (2017) 4693–4701, https://doi.org/10.1016/j.jece.2017.08.024.

[33] F.J. Gutiérrez Ortiz, F. Vidal, P. Ollero, L. Salvador, V. Cortés, A. Giménez, Pilot-plant technical assessment of wet flue gas desulfurization using limestone, Ind. Eng. Chem. Res. 45 (2006) 1466–1477, https://doi.org/10.1021/ie051316o.

[34] A.L. Villanueva Perales, P. Ollero, F.J. Gutierrez Ortiz, A. Gómez-Barea, Model predictive control of a wet limestone flue gas desulfurization pilot plant, Ind. Eng. Chem. Res. 48 (2009) 5399–5405.

[35] J. Zhang, C. You, C. Chen, Effect of internal structure on flue gas desulfurization with rapidly hydrated sorbent in a circulating fluidized bed at moderate temperatures, Ind. Eng. Chem. Res. 49 (2010) 11464–11470.

[36] A. Szymanek, M. de las Obras-Loscertales, A. Pajdak, Effect of sorbent reactivity on flue gas desulphurization in fluidized-bed boilers under air firing mode, Can. J. Chem. Eng. 96 (2018) 895–902.

[37] A.B. Rao, E.S. Rubin, Identifying cost-effective CO2 control levels for amine-based CO2 capture systems, Ind. Eng. Chem. Res. 45 (2006) 2421–2429.

[38] W. Kordylewski, D. Sawicka, T. Falkowski, Laboratory tests on the efficiency of carbon dioxide capture from gases in NaOH solutions, J. Ecol. Eng. 14 (2013).

[39] S. Valluri, S.K. Kawatra, Reduced reagent regeneration energy for CO2 capture with bipolar membrane electrodialysis, Fuel Process. Technol. 213 (2021), 106691.

[40] W. Choi, G. Kim, K. Lee, Influence of the CO2 absorbent monoethanolamine on growth and carbon fixation by the green alga scenedesmus sp, Bioresour. Technol. 120 (2012) 295–299.

[41] A. Goeppert, M. Czaun, G.K.S. Prakash, G.A. Olah, Air as the renewable carbon source of the future: an overview of CO 2 capture from the atmosphere, Energy Environ. Sci. 5 (2012) 7833–7853.

[42] A.A. Mourad, A.F. Mohammad, M. Altarawneh, A.H. Al-Marzouqi, M.H. El-Naas, M.H. Al-Marzouqi, Effects of potassium hydroxide and aluminum oxide on the performance of a modified solvay process for CO2 capture: a comparative study, Int. J. Energy Res. 45 (2021) 13952–13964.

[43] F.A. Awomewe, O.O. Ogundele, The importance of the payback method in capital budgeting decision, Univ. J. Manag. (2008) 1–76.

[45] J. Lim, J. Kim, Optimizing ash deposit removal system to maximize biomass recycling as renewable energy for CO2 reduction, Renew. Energy (2022), https://doi.org/10.1016/j.renene.2022.03.095.

[46] Y. Kim, J. Lim, J.Y. Shim, S. Hong, H. Lee, H. Cho, Optimization of Heat Exchanger Network via Pinch Analysis in Heat Pump-Assisted Textile Industry Wastewater Heat Recovery System, 2022.

[47] J. Lim, H. Lee, H. Cho, J.Y. Shim, H. Lee, J. Kim, Novel waste heat and oil recovery system in the finishing treatment of the textile process for cleaner production with economic improvement, Int. J. Energy Res. (2022) 1–14, https://doi.org/10.1002/er.7803.

[48] Y. Kim, J. Lim, H. Cho, J. Kim, Novel mechanical vapor recompression-assisted evaporation process for improving energy efficiency in pulp and paper industry, Int. J. Energy Res. (2021) 1–19, https://doi.org/10.1002/er.7390.

[49] G. Herz, C. Rix, E. Jacobasch, N. Müller, E. Reichelt, M. Jahn, A. Michaelis, Economic assessment of power-to-liquid processes – influence of electrolysis technology and operating conditions, Appl. Energy 292 (2021), 116655, https://doi.org/10.1016/j.apenergy.2021.116655.

[50] J. Lim, J. Lee, I. Moon, H. Cho, J. Kim, Techno-economic comparison of amine regeneration process with heat-stable amine salt reclaiming units, Energy Sci. Eng. (2021) 1–15, https://doi.org/10.1002/ese3.1000.

[51] J. Lim, J. Lee, H. Cho, J. Kim, Model development of amine regeneration process with electrodialysis reclamation unit, Comput. Aided Chem. Eng. 50 (2021), https://doi.org/10.3390/min7110207.

[52] Anon, in: Proceedings of the International Conference on Stepping Motors and Systems, 1974, 1974, pp. 2118–2121.

[53] M.-R. Yoo, S.-J. Han, J.-Y. Shin, J.-H. Wee, A study on carbon dioxide capture performance of KOH aqueous solution via chemical absorption, J. Korean Soc. Environ. Eng. 34 (2012) 55–62.

[56] M. Madhumala, D. Madhavi, T. Sankarshana, S. Sridhar, Recovery of hydrochloric acid and glycerol from aqueous solutions in chloralkali and chemical process industries by membrane distillation technique, J. Taiwan Inst. Chem. Eng. 45 (2014) 1249–1259.